New Journal of Physics
The open access journal at the forefront of physics

Deutsche Physikalische Gesellschaft DPG
IOP Institute of Physics

Published in partnership with: Deutsche Physikalische Gesellschaft and the Institute of Physics

OPEN ACCESS

RECEIVED
13 November 2017

REVISED
8 March 2018

ACCEPTED FOR PUBLICATION
13 March 2018

PUBLISHED
25 April 2018

PAPER

Non-Markovianity in the optimal control of an open quantum system described by hierarchical equations of motion

E Mangaud[1], R Puthumpally-Joseph[2,3], D Sugny[2,4,8], C Meier[1], O Atabek[5] and M Desouter-Lecomte[6,7,8]

[1] Laboratoire Collisions Agrégats Réactivité (IRSAMC), Universié Toulouse III Paul Sabatier, UMR 5589, F-31062 Toulouse Cedex 09, France
[2] Laboratoire Interdisciplinaire Carnot de Bourgogne (ICB), UMR 6303 CNRS-Université Bourgogne Franche Comté, 9 Av. A. Savary, BP 47 870, F-21078 Dijon cedex, France
[3] Institut des Sciences Moléculaires d'Orsay (ISMO) UMR CNRS 8214, Université Paris Saclay, Univ. Paris Sud, F-91405 Orsay, France
[4] Institute for Advanced Study, Technical University of Munich, Lichtenbergstrasse 2 a, D-85748 Garching, Germany
[5] Institut des Sciences Moléculaires d'Orsay (ISMO) UMR CNRS 8214, Université Paris Saclay, Univ. Paris Sud, F-91405 Orsay, France
[6] Laboratoire de Chimie Physique (LCP)-CNRS, Université Paris Saclay, Univ. Paris Sud, F-91405 Orsay, France
[7] Département de Chimie, Université de Liège, Sart Tilman, B6, B-4000 Liège, Belgium
[8] Authors to whom any correspondence should be addressed.

E-mail: dominique.sugny@u-bourgogne.fr **and** michele.desouter@u-psud.fr

Keywords: optimal control, hierarchical equations of motion, non-Markovianity, fullerene-oligothiophene heterojunction

Abstract

Optimal control theory is implemented with fully converged hierarchical equations of motion (HEOM) describing the time evolution of an open system density matrix strongly coupled to the bath in a spin-boson model. The populations of the two-level sub-system are taken as control objectives; namely, their revivals or exchange when switching off the field. We, in parallel, analyze how the optimal electric field consequently modifies the information back flow from the environment through different non-Markovian witnesses. Although the control field has a dipole interaction with the central sub-system only, its indirect influence on the bath collective mode dynamics is probed through HEOM auxiliary matrices, revealing a strong correlation between control and dissipation during a non-Markovian process. A heterojunction is taken as an illustrative example for modeling in a realistic way the two-level sub-system parameters and its spectral density function leading to a non-perturbative strong coupling regime with the bath. Although, due to strong system-bath couplings, control performances remain rather modest, the most important result is a noticeable increase of the non-Markovian bath response induced by the optimally driven processes.

1. Introduction

Open quantum systems are ubiquitous in physics and chemistry and have many uses from setting quantum technology in condensed phase to exploring long-lived coherence in biological systems [1–6]. They consist in selecting a given partitioning into a central quantum system and a statistical surrounding bath. The reduced system dynamics is non-unitary and can be called Markovian or non-Markovian according to the importance of memory effects [2]. The comparison of system and bath typical timescales is a relevant qualitative measure to separate both situations: if the timescale characterizing the bath is shorter than the one of the system, dynamics can be said Markovian, non-Markovian if not. For a two-level system, this characteristic time is the Rabi period whereas the bath dynamics can be estimated from the time decay of the two-time correlation function of the system bath coupling related to the Fourier transform of the bath spectral density. A nearly delta correlated bath leads to a Markovian behavior usually described by Lindblad [7] or Redfield [2, 5, 8] approaches involving unidirectional relaxation. Non-Markovianity is described by strong quantum memory effects leading to temporary information back flow from the environment to the system. Several measures of non-Markovianity have been proposed and compared recently in the literature [3, 4]. Among them one can mention the distinguishability of quantum states estimated by their trace distance that can transitively decrease during the

relaxation, as opposite to a Markovian evolution in which it continuously increases [9, 10]. Other non-Markovianity signatures refer to a re-amplification of the volume of accessible states during the decay process [11], the detection of a negative canonical decay rate [12, 13], or a non-monotonous time evolution of the system von Neumann entropy [14]. Even more importantly, the role of transitory information back flow in externally controlled dynamics remains an open issue and an active research area [15–31].

Our main purpose is to take advantage of the back flow of information from the surrounding bath, characterizing non-Markovianity, to enforce the control of the central system physical observables, protecting them against decoherence. At that respect, the present paper is a second one of a series of three [29, 30] where an optimal control scheme is worked out, still acting on the central system alone, aiming at some protection against decoherence (population revivals, or robust and efficient transfers) and subsequently examine its consequences in terms of the bath non-Markovian response. More precisely, we analyze non-Markovianity during an ultra-short field pulse optimized by quantum control [32–34] in a spin-boson (SB) model [1, 2, 35] where the active sub-system strongly interacts with the bath. The controlled dynamics ends before the complete decay of the volume of accessible states in the Bloch sphere [11], i.e. before the decay of the bath correlation function which means before quantum memory (or non-Markovian) effects are expected to vanish. The control is also shorter than the full relaxation time of the state populations towards equilibrium. The interaction of the two-level system with the bath is described by the standard SB Hamiltonian which can be used in many different situations ranging from qubit in quantum dots to exciton or charge transfer. In the present work, it is built and calibrated to simulate a charge transfer between donor and acceptor electronic states in a heterojunction [36–38]. The model addresses ultra-short control of electronic dynamics in a complex system strongly coupled to the nuclear vibrational motion [5]. Similar coherent control of excitation energy transfers in photosynthetic systems has already been investigated, but in weak coupling regimes, referring to Markovian approaches [39, 40]. Here we analyze a non-perturbative situation, described through hierarchical equations of motion (HEOM) [41–43, 44–46]. We focus on early dynamics and we investigate the extent to which optimal control field enhances non-Markovianity during control. The canonical decoherence rates and the von Neumann entropy are taken as signatures of non-Markovianity. In a recent work, the enhancement of non-Markovianity during laser driven dynamics has been studied with simple periodic fields in a SB model with a smooth Lorentzian spectral density [25]. This example shows an enhancement of non-Markovianity signatures but for weak coupling only. On the contrary, in the present work, we obtain non Markovian behaviors even in the strongly coupled case.

Optimal control theory (OCT) is implemented here together with the HEOM method. Rabitz monotonous algorithm in Liouville space we are referring to [47–49, 50], requires the forward and the backward propagations of the master equation. The memory kernel occurring in a time non-local master equation with a final condition has been discussed in different works. It has been implemented at second order level keeping the memory kernel [48, 51, 52] and by the auxiliary matrix method leading to time local coupled equations [50, 53]. We generalize here this methodology with HEOM equations at higher order. The HEOM master equation can be rewritten as a time dependent Lindblad superoperator with time dependent canonical rates to get a witness of non-Markovianity [12, 13]. This interesting Krauss decomposition [54, 55] has already been suggested to analyze the control in [20]. In a first attempt, we do not impose any constraint on the field area so that the optimal field is not necessarily an optical one with zero area [56–58, 59]. Such a constraint could be added in a second step, but this issue would go beyond the scope of this paper. The electric field is assumed to have a dipole interaction with the central system only. However, since the memory kernel depends on the external field through the system Hamiltonian, this latter has an influence on the bath dynamics so that control and dissipation are strongly correlated. The modification of the bath dynamics is probed here from the HEOM formalism by analyzing the first moment of the bath collective mode [60].

The paper is organized as follows. Section 2 describes the SB model calibrated from data simulating a charge transfer in a heterojunction. The HEOM equations, the signatures of non-Markovianity and the optimal control theory in dissipative system are presented in section 3. Section 4 gives the results for three ultra-short control cases, two for which the target is the initial state itself (a revival), and one for which the control enforces a transition between the two levels. Finally, some perspectives are presented in section 5.

2. The model

The SB model is a two-level quantum system linearly coupled to a bosonic bath of harmonic oscillators at thermal equilibrium. The Hamiltonian reads

$$H(t) = H_S(t) + H_B + H_{SB}, \tag{1}$$

where $H_S(t) = \delta/2\sigma_z + W\sigma_x - \boldsymbol{\mu}E(t)$, $H_B = \frac{1}{2}\sum_k(p_k^2 + \omega_k^2 q_k^2)$ in mass weighted coordinates and $H_{SB} = S\sum_k c_k q_k$. Atomic units are used with $\hbar = 1$. The system operator is $S = \sigma_z$ with σ_i operators taken as Pauli

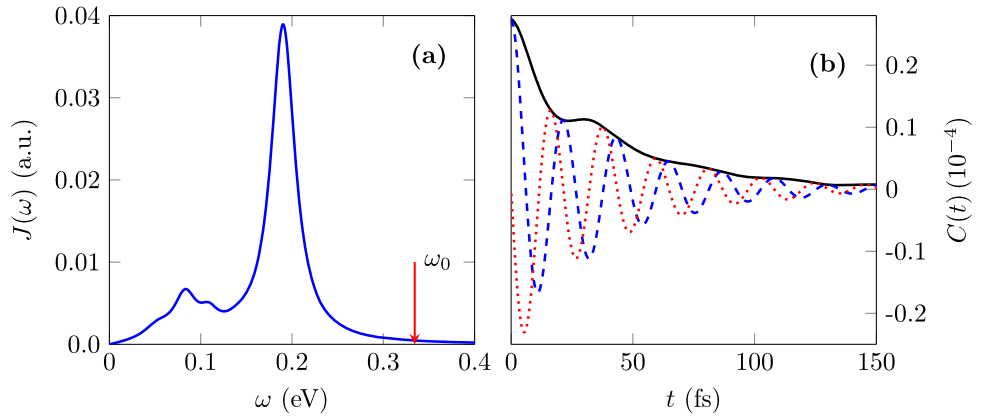

Figure 1. Panel (a): spectral density of the spin-boson model. The red arrow marks the value of the system energy gap. Panel (b): correlation function of the bath mode for $T = 298$ K. The blue dashed curve is the real part and the red dotted curve is the imaginary part of the correlation function $C(t)$. The black solid line is the absolute value of $C(t)$, given in 10^{-4} a.u. units.

matrices. The control field $E(t)$ only acts on the two-level system and is assumed to be linearly polarized. In the context of a charge transfer between a donor and an acceptor in a heterojunction, $H_S(t = 0)$ corresponds to the zero-order or diabatic representation for which the parameters are estimated at the equilibrium geometry. The corresponding eigenstates (namely, $|g\rangle$ and $|e\rangle$) are the delocalized adiabatic electronic states. Starting from $|g\rangle$ and $|e\rangle$, zeroth order site-basis states $|1\rangle$ and $|2\rangle$ are defined as the following coherent superposition:

$$|1\rangle = c_{1g}|g\rangle + c_{1e}|e\rangle \tag{2}$$

and

$$|2\rangle = c_{2g}|g\rangle + c_{2e}|e\rangle. \tag{3}$$

Such site-states still remain coupled through an interstate potential coupling W. The diabatic parameters δ and W are taken from a model heterojunction between oligothiophene and fullerene [36, 37]. The inter fragment distance is fixed to $R = 3$ Å leading to $\delta = 0.21$ eV and $W = 0.13$ eV. The corresponding Rabi period is 12.3 fs and the eigenenergy gap is 0.33 eV. The $\boldsymbol{\mu}$ matrix is the matrix of the dipole operator in the zero-order basis set. The dipole matrices are not calibrated from *ab initio* calculations and different dipole models have been used to discuss the stability of the observed behaviors. In this electron transfer framework, the bath is formed by all the normal modes of the two fragments, taken as 264 in the present model. The harmonic frequencies are assumed to be the same in both electronic states but the equilibrium geometries differ by a distance d_k. Taking the origin of bath coordinates at a middle position between these equilibrium points, the vibronic coupling coefficients are $c_k = \omega_k{}^2 d_k/2$.

The bath is fully characterized by the spectral density

$$J(\omega) = \frac{\pi}{2}\sum_k \frac{{c_k}^2}{\omega_k}\delta(\omega - \omega_k) \tag{4}$$

leading to the two-time correlation function

$$C(t-\tau) = \mathrm{Tr}_B[B(t)B(\tau)\rho_B^{\mathrm{eq}}] = \frac{1}{\pi}\int_{-\infty}^{+\infty} \mathrm{d}\omega \frac{J(\omega)\mathrm{e}^{\mathrm{i}\omega(t-\tau)}}{\mathrm{e}^{\beta\omega} - 1}, \tag{5}$$

where $B(t) = \exp(\mathrm{i}H_B t)B\exp(-\mathrm{i}H_B t)$ is the bath operator $B = \sum_k c_k q_k$ in the Heisenberg representation. $\rho_B^{\mathrm{eq}} = \exp(-\beta H_B)/\mathrm{Tr}_B[\exp(-\beta H_B)]$ is the Boltzmann equilibrium density matrix of the bath and $\beta = 1/k_B T$. Spectral density and correlation functions (real, imaginary parts and modulus) of this heterojunction model are displayed in figure 1. In this example, the Rabi period (12.3 fs) is smaller than the correlation time (25 fs) so that non-Markovian dynamics is expected.

As displayed in figure 1, the spectral density $J(\omega)$ is fitted by four four-pole functions

$$J(\omega) = \sum_{l=1}^{4} \frac{p_l \omega^3}{\Lambda_{l,1}(\omega)\,\Lambda_{l,2}(\omega)}, \tag{6}$$

where

$$\Lambda_{l,(1,2)}(\omega) = [(\omega + \Omega_{l,(1,2)})^2 + \Gamma_{l,(1,2)}^2][(\omega - \Omega_{l,(1,2)})^2 + \Gamma_{l,(1,2)}^2]. \tag{7}$$

Cauchy's residue theorem is used to compute the integral of equation (5) with a contour closed in the upper half-plane enclosing $4n_l$ poles in $(\Omega_{l,1}, \Gamma_{l,1})$, $(-\Omega_{l,1}, \Gamma_{l,1})$, $(\Omega_{l,2}, \Gamma_{l,2})$, $(-\Omega_{l,2}, \Gamma_{l,2})$ and an infinity of poles on the

imaginary axis $\left\{\forall j \in \mathbb{N}^* \Big/ \left(0,\ \nu_j = \frac{2\pi}{\beta} j\right)\right\}$ called the Matsubara frequencies. In practice, the number of Matsubara terms is limited ensuring convergence for a given temperature.

3. Methods

3.1. HEOM equations

The system density matrix is the partial trace of the full density matrix $\Xi(t)$ over the bath degrees of freedom $\rho(t) = \mathrm{Tr}_B[\Xi(t)]$. As a first approximation, the initial condition is assumed to be factorized as:

$$\Xi(t=0) = \rho(t=0)\rho_B^{\mathrm{eq}}. \tag{8}$$

This assumption is fully valid only for fast bath response leading to Markovian dynamics, or at least for weakly coupled systems. Initial correlation is expected to modify the dissipative dynamics and witnesses of such initial entanglement have also been discussed [3, 4, 61–63]. This important issue has been addressed by different methods, for instance in Multi Configuration Time Dependent Hartree approach [64], second order auxiliary matrices [65] or HEOM methodology [43, 66] which leads to an interesting strategy taking partially into account initial correlations, as is briefly discussed hereafter.

HEOM equations have been established from the path integral method [44] or from the stochastic Liouville equation [41–43]. The non-Markovian master equation

$$\dot{\rho}(t) = -\mathrm{i}\mathrm{Tr}_B([H,\ \Xi(t)]) \tag{9}$$

is solved by a time local system of coupled equations among auxiliary matrices arranged in a hierarchical structure. The algorithm requires a particular parametrization of the correlation function as a sum of n_{cor} exponential terms, written as:

$$C(t-\tau) = \sum_{k=1}^{n_{\mathrm{cor}}} \alpha_k \mathrm{e}^{\mathrm{i}\gamma_k(t-\tau)}. \tag{10}$$

Analytical expressions for the α_k and γ_k parameters can be derived when the spectral density is fitted by a sum of two-poles [67] or four-pole Lorentzian functions leading to an Ohmic or super Ohmic behavior at low frequencies [38]. The complex conjugate of the correlation function can be expressed by keeping the same coefficients γ_k in the exponential functions but using modified coefficients $\tilde{\alpha}_k$ according to:

$$C^*(t-\tau) = \sum_{k=1}^{n_{\mathrm{cor}}} \tilde{\alpha}_k \mathrm{e}^{\mathrm{i}\gamma_k(t-\tau)} \tag{11}$$

k being a collective index such that, $\tilde{\alpha}_{l,1} = \alpha^*_{l,2}$, $\tilde{\alpha}_{l,2} = \alpha^*_{l,1}$, $\tilde{\alpha}_{l,3} = \alpha^*_{l,4}$, $\tilde{\alpha}_{l,4} = \alpha^*_{l,3}$ and $\tilde{\alpha}_{j,\mathrm{matsu}} = \alpha_{j,\mathrm{matsu}}$, where $\alpha_{l,m}$, $\tilde{\alpha}_{l,m}$ with $m = 1, 4$ are related to the four poles of each Lorentzian l [65].

The level L of the hierarchy corresponds to an order $2L$ in the perturbation expansion of the initial non-Markovian equation. Auxiliary matrices are labeled by a collective index $\mathbf{n} = \{n_1, \cdots, n_{n_{\mathrm{cor}}}\}$ specifying the number of occupation of each artificial mode associated with one of n_{cor} decaying components. The system density matrix $\rho(t)$ has the index $\mathbf{n} = \{0, \cdots, 0\}$. The first level $L = 1$ contains n_{cor} auxiliary matrices with a single excitation only $\sum_k n_k = 1$. The HEOM coupled differential equations are given by:

$$\begin{aligned}\dot{\rho}_{\mathbf{n}}(t) = &-\mathrm{i}[H_S(t),\ \rho_{\mathbf{n}}(t)] + \mathrm{i}\sum_{k=1}^{n_{\mathrm{cor}}} n_k\gamma_k\rho_{\mathbf{n}}(t) \\ &- \mathrm{i}\left[S,\ \sum_{k=1}^{n_{\mathrm{cor}}}\rho_{\mathbf{n}_k^+}(t)\right] - \mathrm{i}\sum_{k=1}^{n_{\mathrm{cor}}} n_k(\alpha_k S\rho_{\mathbf{n}_k^-} - \tilde{\alpha}_k\rho_{\mathbf{n}_k^-}S)\end{aligned} \tag{12}$$

with $\mathbf{n}_k^+ = \{n_1, \cdots, n_k + 1, \ldots, n_{n_{\mathrm{cor}}}\}$ and $\mathbf{n}_k^- = \{n_1, \cdots, n_k - 1, \ldots, n_{n_{\mathrm{cor}}}\}$. Each matrix is coupled only to the superior and inferior levels in the hierarchy. The level of the hierarchy is chosen until convergence is reached for the system density matrix.

The HEOM formalism allows one to get insight into the correlated system-bath dynamics by probing the different moments $X^{(n)}(t) = \mathrm{Tr}_B[B^n\Xi(t)]$ of the collective mode $B = \sum_i c_i q_i$ [60]. In particular, the expectation value of B in each state is given by the diagonal elements of the $X^{(1)}(t)$ operator given by the sum of the first level auxiliary matrices

$$X^{(1)}(t) = -\sum_{\mathbf{n}} \rho_{\mathbf{n}}(t), \tag{13}$$

where the sum runs over all index vectors $\mathbf{n} = \{n_1, \cdots, n_{n_{\mathrm{cor}}}\}$ with $\sum_l n_l = 1$. Recursive formula for higher orders can be found in [60]. This first moment already provides a signature of the induced correlated system-bath dynamics. As discussed in [60], the master equation can be recast to emphasize the role of $X^{(1)}(t)$ in the system dynamics by writing

$$\dot{\rho}(t) = -\mathrm{i}[H_S,\, \rho(t)] + \mathrm{i}[S,\, X^{(1)}(t)]. \tag{14}$$

Assuming system-bath separability equation (8), auxiliary matrices are set equal to zero at initial time. An improvement to account for initial system-bath correlation consists in propagating in field-free conditions up to equilibrium, i.e. for times much longer than the bath correlation time [66]. The resulting state is in principle a partially coherent superposition of the system and the bath. The equilibrated auxiliary matrices are then used to describe initial conditions, while the system density matrix is set to a specific initial state.

3.2. Non-Markovian witnesses

Signature of non-Markovianity is discussed here through the volume of accessible states [11] and through the canonical decoherence rates of a time-dependent Lindblad form [12, 13]. In the two-level case, the dynamical map $\rho(t) = \phi_t[\rho(0)]$ is first expressed in the basis set of the d^2 Hermitian operators (here $d = 2$) formed by the identity $G_0 = \mathbf{I}/\sqrt{d}$ and three operators G_m with $m = 1, 3$ which are the Pauli matrices $\sigma_{x,y,z}/\sqrt{d}$. The equation then becomes

$$\rho(t) = \sum_{k=0}^{d^2-1} \mathrm{Tr}(G_k \rho(0))\, \phi_t[G_k]. \tag{15}$$

The volume of accessible states may be obtained from the matrix representation of the dynamical map in this basis set $F_{m,n}(t) = \mathrm{Tr}(G_m \phi_t[G_n])$ by

$$V(t) = \det(\mathbf{F}). \tag{16}$$

This volume may also be expressed as a function of the decoherence canonical rates. The master equation is then recast in a canonical Lindblad form but with time dependent rates associated with time-dependent decay channels. Details can be found in [12, 13]. The master equation is reformulated as

$$\dot{\rho}(t) = -\mathrm{i}[H_S,\, \rho(t)] + \sum_{j,k=0}^{d^2-1} a_{jk}(t)\, G_j \rho(t) G_k. \tag{17}$$

In order to describe the decrease of the Bloch volume independently of the translation of its center, the contribution of the unity operator is separated by gathering terms containing coefficients a_{j0}. One then defines an operator $O = a_{00}/2d + \sum_{i=1}^{d^2-1}(a_{i0}/d^{1/2}) G_i$ and a corrected system Hamiltonian $H_{S\,\mathrm{cor}} = \mathrm{i}(O - O^\dagger)/2$. The relaxation operator then involves only the three operators associated with the Pauli matrices and the master equation takes the form:

$$\dot{\rho}(t) = -\mathrm{i}[H_{S\,\mathrm{cor}},\, \rho(t)] + \sum_{j,k=1}^{d^2-1} D_{jk}(t)\left(G_j \rho(t) G_k - \frac{1}{2}\{G_k G_j,\, \rho(t)\} \right), \tag{18}$$

where $D_{jk}(t)$ is the decoherence matrix. Its diagonalization provides the decoherence canonical rates $g_k(t)$ and the decay channels $C_k(t)$. Equation (18) becomes

$$\begin{aligned} \dot{\rho}(t) = &-\mathrm{i}[\hat{H}_{\mathrm{Scor}},\, \rho(t)] \\ &+ \sum_{k=1}^{d^2-1} g_k(t)(2C_k(t)\rho(t)C_k^\dagger(t) - \{C_k^\dagger(t)C_k(t),\, \rho(t)\}), \end{aligned} \tag{19}$$

with $D_{ij}(t) = \sum_{k=1}^{d^2-1} U_{ik}(t) g_k(t) U_{jk}^*(t)$ and $C_k(t) = \sum_{i=1}^{d^2-1} U_{ik}(t) G_i$.

It is worthwhile noting that the occurrence of negative canonical decoherence rates $g_k(t)$ yields another characterization of non-Markovianity [12]. The rates are linked to the volume of accessible states through the relation

$$V(t) = V(0) \exp\left(-\mathrm{d} \int_0^t \Gamma(s)\mathrm{d}s \right), \tag{20}$$

with

$$\Gamma(t) = \sum_{k=1}^{d^2-1} g_k(t). \tag{21}$$

The criterion based on the volume can be considered as an average measure since it depends on the sum of the rates only. Thus, it can be considered as a less stringent witness of non-Markovianity than a negative canonical decoherence rate $g_k(t)$.

A possible numerical strategy to compute the decoherence matrix $D_{ij}(t)$ has been discussed in [12] and is given by

$$D_{ij}(t) = \sum_{m=0}^{d^2-1} \mathrm{Tr}[G_m G_i \Lambda_t[G_m] G_j] \tag{22}$$

with

$$\Lambda_t[G_j] = \sum_{k=0}^{d^2-1} \dot{\phi}_t[G_k] F_{kj}^{-1}. \tag{23}$$

Besides the analysis of the decoherence canonical rates, we also compute the von Neumann entropy of the system that should vary monotonously in a Markovian evolution [14]

$$S(\rho(t)) = -\mathrm{Tr}[\rho(t)\log_2 \rho(t)] = -\sum_k \lambda_k \log_2 \lambda_k, \tag{24}$$

where λ_k are the eigenvalues of the system density matrix.

3.3. Optimal control theory

We use optimal control theory in the Liouville space [47, 48, 50] to optimize the field driven state-to-state transfer at the end of the pulse of total duration t_f. The cost functional $\mathcal{F}$ to be minimized is built from a chosen performance index $\langle \rho(t_f)|\rho_{\mathrm{target}}\rangle = \mathrm{Tr}[\rho^\dagger(t_f)\rho_{\mathrm{target}}]$ together with two constraints, namely on the field strength and on the fulfillment of the master equation at any time. More specifically $\mathcal{F}$ is given as:

$$\begin{aligned}\mathcal{F} = \langle \rho(t_f)|\rho_{\mathrm{target}}\rangle &- \alpha_0 \int_0^{t_f} \Delta E(t)^2 \mathrm{d}t \\ &- 2\Re\left[\langle \rho(t_f)|\rho_{\mathrm{target}}\rangle \int_0^{t_f} \langle \chi(t)|\partial\rho/\partial t + \mathrm{i}[H_S, \rho]\rangle \mathrm{d}t\right].\end{aligned} \tag{25}$$

The corresponding Lagrange multipliers are the scalar α_0 and the density matrix $\chi(t)$ respectively. However, we do not use the procedure, for instance presented in [68], to modify the parameter during the optimization in order to precisely control the total final intensity. We have merely stopped the control iterations when the field amplitude reaches about 0.01 a.u. (see figure 2, panels (d)–(f)). This roughly corresponds to leading intensities less than 3×10^{12} W cm^{-2}, which are considered to be not too strong. We do not enforce here the constraint on the zero pulse area which is required for a purely optical field [59]. The aim, for this first attempt, is to obtain the maximum efficiency that could be expected from the control process. The optimal field is obtained from the system density matrix propagated by the master equation with initial condition $\rho(t=0) = \rho_{\mathrm{ini}}$ and from the Lagrange multiplier propagated with a final condition $\chi(t=t_f) = \rho_{\mathrm{target}}$. The corresponding master equations with initial and final conditions take the form with $L\bullet = -\mathrm{i}[H_S(t), \bullet]$

$$\dot{\rho}(t) = L\rho(t) + \int_0^t K(t, t')\rho(t')\mathrm{d}t' \tag{26}$$

$$\dot{\chi}(t) = L\chi(t) - \int_t^{t_f} K^\dagger(t, t')\chi(t')\mathrm{d}t'. \tag{27}$$

It is worthwhile noting that these equations lead to a correlation between control and dissipation since the Liouvillian and the memory kernel K in equations (26, 27) take into account the external control field, even though, in our model, dipole interaction is solely acting within the central system [50, 67].

When the master equation is solved by the HEOM algorithm, the operational equations for the Lagrange multiplier can be derived by using equations (10) and (11)

$$\begin{aligned}\dot{\chi}_{\mathbf{n}}(t) = L\rho_{\mathbf{n}}(t) &- \mathrm{i}\sum_{k=1}^{n_{\mathrm{cor}}} n_k\gamma_k\rho_{\mathbf{n}}(t) \\ &- \mathrm{i}\left[S, \sum_{k=1}^{n_{\mathrm{cor}}} \rho_{\mathbf{n}_k^+}(t)\right] + \mathrm{i}\sum_{k=1}^{n_{\mathrm{cor}}} n_k(\alpha_k\rho_{\mathbf{n}_k^-}S - \tilde{\alpha}_k S\rho_{\mathbf{n}_k^-}).\end{aligned} \tag{28}$$

In practice equation (28) is solved backwards starting from $\chi_{\{0,0,\ldots,0\}}(t=t_f) = \rho_{\mathrm{target}}$. Within the initial factorization approximation, the auxiliary matrices are set equal to zero for both initial and target states. We have checked that the coupled OCT-HEOM algorithm remains stable when starting from the auxiliary matrices obtained by propagating the initial state up to equilibrium. However, a detailed analysis of the control process with initial correlation, goes beyond the scope of this manuscript, and should be addressed in future works.

The field at iteration k is obtained by $E^{(k)} = E^{(k-1)} + \Delta E^{(k)}$, where $\Delta E^{(k)}$ is estimated by [47]:

$$\Delta E(t) = \frac{1}{\alpha_0}\Im m\{\mathrm{Tr}(\rho(t)\chi(t))\mathrm{Tr}(\chi(t)[\boldsymbol{\mu}, \rho(t)])\}. \tag{29}$$

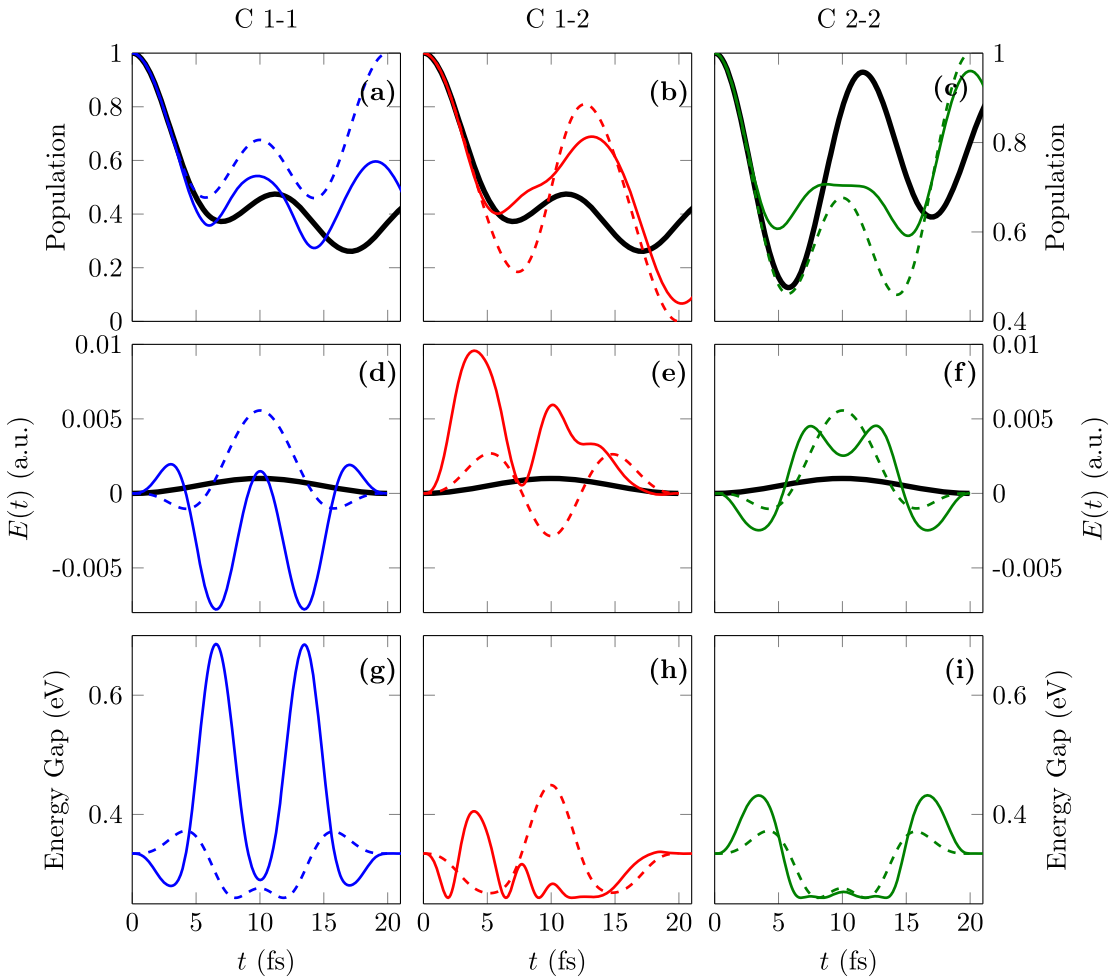

Figure 2. The three columns correspond to the three control strategies: C1-1, C1-2 and C2-2 respectively. Upper panels: evolution of the population in the initial state (black full line: field-free dynamics, colored full lines: OCT with dissipation, dashed lines: OCT without dissipation). Middle panels: amplitude of the electric fields (black solid line: guess field, colored full lines: optimal field with dissipation, dashed lines: optimal field without dissipation). Lower panels: fluctuations of the instantaneous system eigenenergy gaps $\omega_0(t)$ induced by the corresponding optimal fields (full lines: OCT with dissipation, dashed lines: OCT without dissipation).

4. Results

HEOM equations are solved using a Cash–Karp adaptative stepsize Runge–Kutta algorithm with a small time step of 2 a.u. during which the field is assumed to be constant. Dynamics converges at level $L = 6$ of the HEOM hierarchy, i.e. at order 12 in perturbation theory which shows a strong system-bath coupling. In the above examples the dipole matrix is merely set equal to $\boldsymbol{\mu} = \mu\sigma_z$ with $\mu = 1$ a.u. It is worthwhile noting that the diagonal structure of the dipole matrix is merely due to its representation in the zeroth order diabatic basis. Off-diagonal elements would result when going to its adiabatic eigenbasis set representation. Stability of the results has been verified for different non diagonal dipole matrices. The guess field is a sine square with maximum amplitude 10^{-3} a.u. The duration of the control is fixed to 20 fs, smaller than typical times for the complete field free decay of the Bloch sphere volume (equation (16)). No constraint on the shape of the field is imposed by the OCT algorithm, except a penalty factor in such a way that the field amplitude does not exceed 10^{-2} a.u. (3.51×10^{12} W cm^{-2}).

4.1. Field-controlled dynamics

We consider three control objectives defined by the populations of the system. In the two first strategies that are denoted C1-1 and C2-2, the target is the revival of initial zero-order state, either state $|1\rangle$ or $|2\rangle$, at the end of the control. We recall that these site-states are coherent superpositions of some ground and excited states of the heterojunction modeled as a donor-acceptor dimer (see equations (2) and (3)). A third control denoted C1-2, enforces the fast decay from state 1 to state 2 (a fast switch from 1 to 2). We compare the control without or with dissipation and analyze both the system and bath responses (memory effects) during the corresponding field-driven dynamics.

The field-free and field-driven populations in the initial state during the three control strategies are shown in the upper panels (a)–(c) of figure 2. The field free evolution (full black lines in figure 2) displays the expected damped Rabi oscillations of 12.3 fs. The dashed lines in panels (a) for C1-1, (b) for C1-2 or (c) for C2-2 are the populations driven by the optimal fields without dissipation. The objective is then reached easily with a performance index of 1. When the system is coupled to the bath, the populations are the full lines (blue for C1-1, red for C1-2 and green for C2-2). Panel (a) shows, for C1-1 strategy, at almost all times (except between 12 and 15 fs) a field enhanced protection of the population of the initial state 1 resulting in about 10% of increase at the end of the control with respect to the field-free case. Similar final results are obtained for C2-2 illustrated in panel (b) and C1-2 (panel (c)) but their final results nearly match their dedicated target. In the isolated system, the only possible mechanism should be a modification of the oscillation periods, a decrease in the C1-1 or C2-2 scenario and an increase in the C1-2 case. This can be related to the transient variation of the energy gap induced by the control. In presence of dissipation, the variation of the gap acts both on the period and on the strength of the system-bath coupling. Panels (d)–(f) in figure 2 present the corresponding optimal fields for control with and without dissipation. It is worthwhile noting that field profiles are very symmetrical for the two control strategies C1-1 and C2-2. This observation is merely in relation with the structure of the evolution algorithm involving an initial condition (for the forward propagation) identical to the final one (for the backward propagation). The control scenario C1-2, illustrated in the middle panels of figure 2, is aiming at the enhancement of the population of level 2, when level 1 is taken as an initial state (i.e. different initial and target states). The field-free energy gap is 0.33 eV and the optimal fields induce different Stark shifts in a range of about 0.25–0.65 eV, so that the instantaneous resonance frequency $\omega_0(t)$ moves with respect to the spectral density peaks, with its expected consequences on non-Markovianity [29, 30]. Obviously, different initial states, with different field-free energy gaps (characterizing heterojunction models with different inner-fragment distances [38]) will result into different control parameters, but still with transposable strategies and generic enough results. The fluctuations of the eigenenergy gap of the field-dressed system Hamiltonian are shown in panels (g)–(i) of figure 2. Convergence has been checked by changing the sign of the initial field: this leads to nearly the same final shape of the optimal fields. The mechanism found by the control exploits transitory decrease of the energy gap leading to a region where the coupling with the bath increases and transitory strong increase of the gap leading to a decrease of the bath coupling but probably an enhancement of non-Markovian effects.

Obviously, control performances remain rather modest. This point can be explained both by limitations of the control parameters (rather low field amplitudes and short pulse duration), and more importantly, by the way the strong system-bath interactions inherent to the specific molecular situation at hand interplays with the control. This can be numerically rationalized through the analysis of the first moment of the bath collective mode in each state given by the diagonal elements of the (2×2) $X^{(1)}$ matrix as depicted in equation (13). Although the control only acts on the system Hamiltonian, it affects the overall dynamics through the memory terms included in the right-hand-side of equation (12). Control fields indirectly modify the bath response leading to a strong correlation between control and dissipation. This is illustrated in figure 3 which displays the first moment of the bath collective mode, in terms of the diagonal elements $X^{(1)}_{1,1}$ (left column) and $X^{(1)}_{2,2}$ (right column), starting either from initial state 1 (upper line) or 2 (lower line). The first observation is that bath oscillations roughly follow the field-driven modifications of the Rabi period, with some amplitude and period variations. But marked differences are depicted according to the initial state. For initial state 1, the short time dynamics (up to about 5 fs) is such that the field-controlled bath motions follow their field-free counterparts. Discrepancies from the field-free behaviors occur with opposite signs for $X^{(1)}_{1,1}$ and $X^{(1)}_{2,2}$, starting from the time when the gap is at its maximum value, i.e. close to 6 fs for C1-1 and 4 fs for C1-2 control strategies. Actually, when dealing with these two strategies, the gap is decreasing during the first femtoseconds, such that the system internal transition frequencies better match bath resonant phonons transitions. As a consequence, the amplitudes of collective modes oscillations are expected to increase. For initial state 2 and the corresponding C2-2 control strategy, early Stark shifts have an opposite sign leading to increasing gaps, preventing bath resonant processes from occuring. Discrepancy from the field-free situation occurs at the very beginning of the control process. Such observations on the first moment $X^{(1)}$ can be considered as additional insights for a comprehensive rationalization of control strategies as they evolve in time. Actually, it turns out that control fields take advantage from two simultaneous mechanisms: (i) population transfer improved by modifying the Rabi frequency, through the Stark shift directly affecting the central system; (ii) dynamical decoupling effects, through indirect processes in the bath, preventing overall decoherence. It is worthwhile noting that, we have previously reported similar mechanisms with single cycle or dc fields [30]. As a final comment, these mechanisms being dynamically mixed, a non-Markovian diagnostic cannot merely be inferred from their analysis. This motivates the need to resort to other non-Markovian witnesses as is done hereafter.

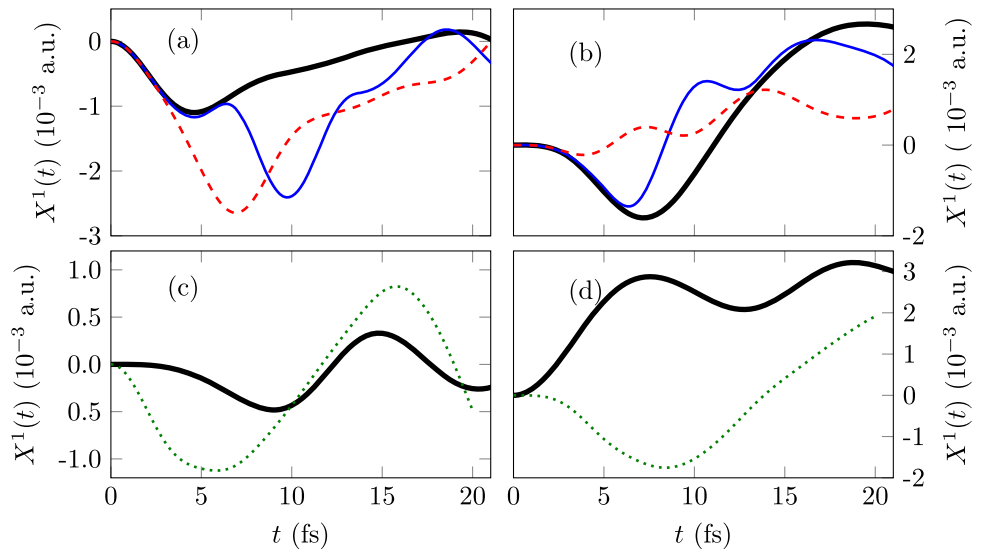

Figure 3. Evolution of the diagonal elements of the $X^{(1)}(t)$ operator giving the first moment of the bath collective mode. Left panels ((a) and (c)) for $X^{(1)}_{1,1}$ and right panels ((b) and (d)) for $X^{(1)}_{2,2}$. Upper panels, for initial state 1: field-free in full black lines, control C1-1 in full blue lines and C1-2 in dashed lines. Lower panels, for initial state 2: field-free in full black lines, control C2-2 in dotted lines.

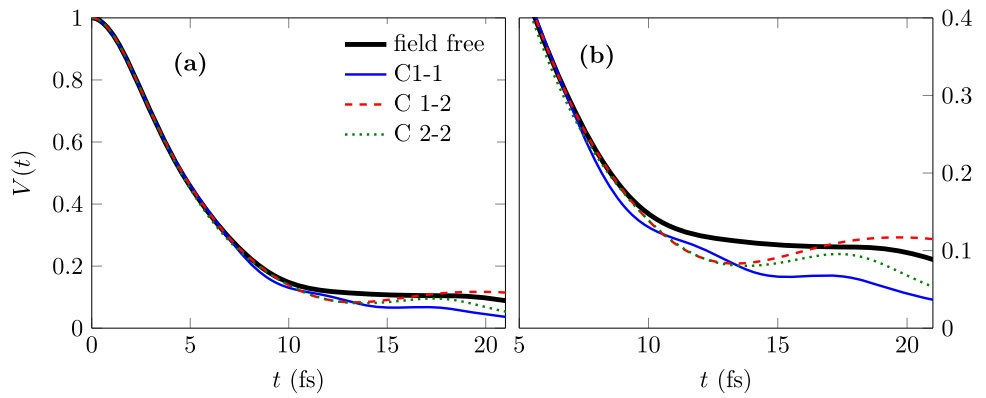

Figure 4. Panel (a): volume (dimensionless) of accessible states for field-free (solid black line) or field-controlled dynamics using strategies C1-1 (solid blue line), C2-2 (dotted green line) and C1-2 (dashed red line). Panel (b) is a zoom of (a) for times larger than 5 fs.

4.2. Non-Markovian signatures

During the field-free evolution, the volume of accessible states illustrated in figure 4 decreases very fast, in about 30 fs with a smooth monotonous decreasing profile. Nevertheless the decay is not exponential as it should be in a Markovian process. The duration of the control is fixed to 20 fs, i.e. less than the time for a complete decay of the volume. The resulting behaviors are displayed with the three control strategies C1-1, C2-2 and C1-2. Basically, after 5 fs, the decay is slightly faster than the field-free case and, more importantly, one observes some bumps, considered as clear signatures of non-Markovianity. Actually, the bumps arise at times close to 12 fs (for C1-1) or 17 fs (for C2-2) which could be associated with the maxima of the Stark shifts affecting the system energy gaps as displayed in figure 2. As shown in equation (16), this volume can also be computed from the sum of the canonical rates which are the eigenvalues of the decoherence matrix. This sum (equation (21)) displayed in figure 5 clearly shows the increase of non-Markovianity during the controlled evolution. More precisely, negative values for $\Gamma(t)$, responsible for the bumps of the volume, occur between 12 and 17 fs, mainly with the C2-2 and C1-2 control strategies. It is worthwhile noting the relation with important Stark shift affecting the system at such times as seen on figure 2. These analyses conclude that the field-dressed dynamics during the optimal control is more non-Markovian than the field-free evolution. Moreover, one may question about the particular role of the quantum channel with the negative rate that should correspond to some backward flow. In order to observe the role of the different decoherence channels (equation (19)) during the evolution of a given initial state, we compute the weight of the three quantum channels as:

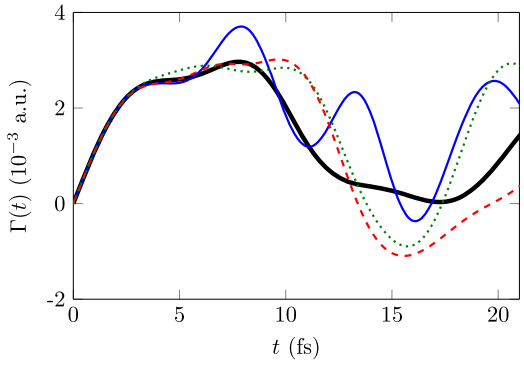

Figure 5. Sum of the canonical decoherence rates (equation (21)) for the field-free (thick solid black line) and controlled system: thin solid blue for C1-1, dotted green for C2-2 and dashed red for C1-2.

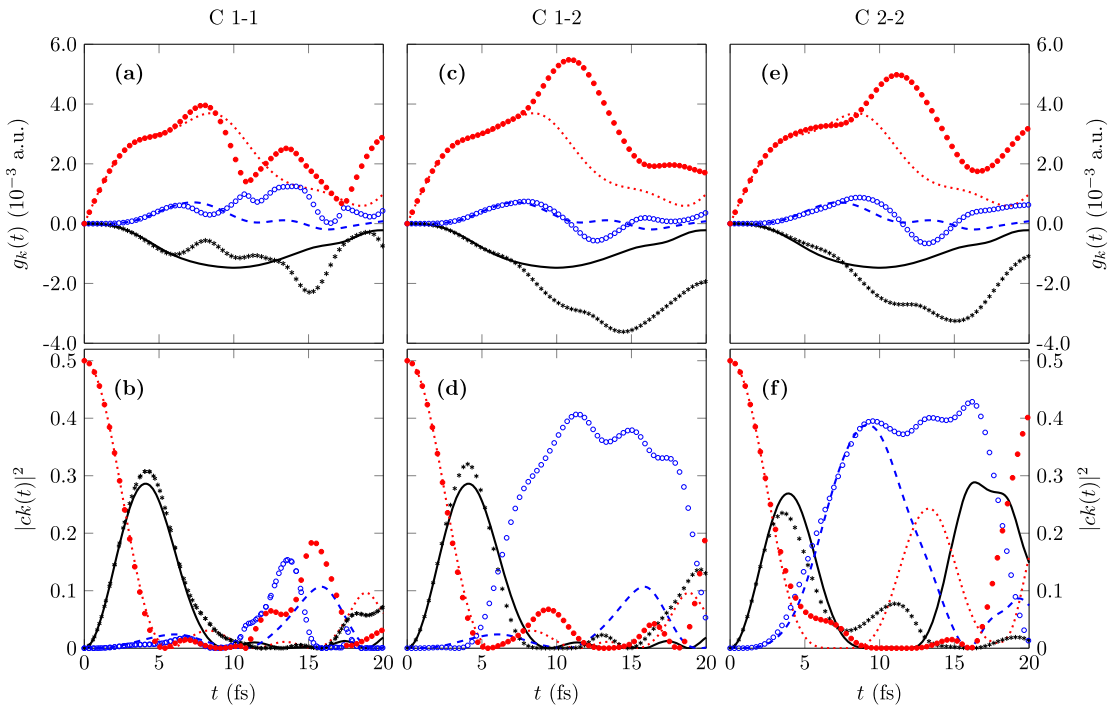

Figure 6. Panel (a): canonical rates (equation (19)) for the field-free (solid black $k = 1$, dashed blue $k = 2$ and dotted red $k = 3$ lines) and field-controlled (black stars, blue thin circles and red thick circles) evolution during the three control strategies. The rates are given in ascending order. Panel (b): weights of the decoherence channels $c_k(t)$ during the same evolution.

$$c_k(t) = \mathrm{Tr}[C_k^\dagger(t)\rho(t)]. \tag{30}$$

Note that the operator G_0 (corresponding to the unity matrix) is not involved in the computation of coherence matrices so that the initial sum of $|c_k(t=0)|^2$ is equal to 0.5 and this sum is not conserved during the evolution since the decoherence matrix only describes the decrease of the volume and not its translation in the Bloch sphere. The upper panels of figure 6 show the three canonical rates during the field-free and field-controlled evolutions. The rates are given in increasing order so that channel $k = 1$ corresponds to the negative rate, which may become even more negative during the control as seen in panels (c) and (e) after 7 fs during controls C1-2 and C2-2. The lower panels present the weights $|c_k(t)|^2$ during the relaxation. This illustrates the different impact of the negative rate during the control. The main observations are the following: (i) the weights of channel $k = 1$ with the most negative rates (black stars) always dominate around 5 fs but become the lowest after 8 fs except at the end of controls C1-1 and C2-2; (ii) the leading channel after 8 fs is $k = 2$ associated with the smallest positive rates (blue curves) during C2-2 and C1-2. It decreases with respect to the field-free case at the end of the C2-2 strategy; (iii) the highest positive rates are increased by the control fields, but more importantly their weights may decrease, for instance in the range 10–15 fs during control C2-2. As a consequence, the effective decay rate is basically affected by the combination of these effects. The increase of non-Markovianity during control does not necessarily imply that the channel with the negative rate plays the most significant role. In other words, an

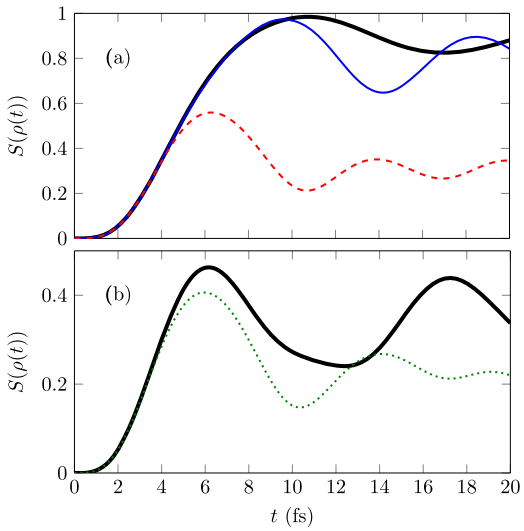

Figure 7. System entropy during the field-free (solid lines) or field-controlled dynamics (dashed and dotted lines). Panel (a): initial state 1, where dashed blue dashed line is for the control strategy C1-1 and red dotted line is for C1-2. Panel (b): same as (a) but for the initial state 2 (control C2-2).

efficient control strategy for enforcing the bumps in the volume evolution, cannot merely be the tracking at each time of the channel with the negative partial rate, as it could be expected.

The volume of reachable states is a global property of the system. It is built from the dynamical map so that when it exhibits non-Markovian witness, it is expected that similar signatures could be found in properties related to the evolution of a particular initial state. As already discussed [14], non-Markovian witness can be seen in the system entropy (equation (24)) shown in figure 7. The Markovian evolution of the entropy when the initial state is a pure state should be a monotonous evolution towards the value associated to the final Boltzmann mixture. In the present case, due to the energy gap, the final state is nearly the ground eigenstate so that the entropy profile should be a monotonous bell shape function. The non-Markovian signature is linked to any local decrease in the entropy which corresponds to a similar local bump in the purity $\mathrm{Tr}(\rho^2(t))$ and therefore to an enhancement of the coherence. For instance, such a non-Markovian information back flow occurs between 11 fs and 18 fs in the field-free evolution of state 1 and between 6 fs and 12 fs for state 2 (black curves). One observes that the dressed dynamics enhances this effect and more interestingly reduces the maximum entropy in a given time interval as during the control 1 to 2 (red dots in figure 7).

The previous analysis concerns a time control close to the bath correlation time for which complete relaxation is still not reached, since this would require about 200 fs. We have checked, for the C1-1 control, longer pulse durations, 50 fs and 100 fs respectively, by choosing the same sine-square guess field, with a maximum amplitude of 0.001 a.u. and compared the optimal control result after 200 iterations. For the 50 fs pulse, the optimal field maximum amplitude remains similar to that of the 20 fs one, but it is twice smaller for the 100 fs pulse. After 200 iterations, the total pulse intensity is not the same so that one should be careful when carrying out such a comparison. The optimization performances are similar. Nevertheless, we observe an unexpected better result for the 50 fs case that uses a different mechanism in comparison to the one we have discussed in this work. As the pulse has mostly positive amplitudes, we assume that a different mechanism from the one we have discussed in this work is at stake. However the results contain most of the physics we want to exhibit: (1) the non-Markovian witnesses qualitatively behave as during the short control. The studied system is strongly non-Markovian as can be seen in the field-free case from the transitory negative sum of the canonical rates well after the bath correlation time as shown in [38]. (2) The field driven dynamics exploits the non-Markovian character of the bath well beyond the bath correlation time. (3) The optimal pulse profile and its induced Stark shift depend on the pulse duration: different mechanisms can be found by the optimal control algorithm. The temporary decrease or increase of the Rabi period shows that it can be a balance between a dynamical decoupling mechanism and the use of non-Markovian effects. The 20 fs control presented here, although typical with respect to all the qualitative behaviors, is not the unique route found by the OCT algorithm.

We have checked on the C1-1 control case that taking into account initial correlation slightly modifies the dynamics, for instance the amplitude of the damped Rabi oscillation during the field-free evolution. However, the control mechanism remains qualitatively similar leading to comparable Stark shift. A deeper analysis is necessary to generalize the conclusions, in particular to examine whether initial correlation could better protect

coherence (i.e. longer lasting entanglement) as observed when properly describing the initial state [66]. The control efficiency could possibly be slightly improved, but at least not deteriorated. This important development is currently in prospect.

5. Conclusion

This work is devoted to a detailed analysis of external field control versus dissipation in non-Markovian strongly coupled open quantum systems. A heterojunction is taken as an illustrative example with its specific parameters and spectral density, building up a SB type Hamiltonian. With respect to methodology, the originality relies on a complete implementation of an optimal control scheme, together with a fully converged HEOM treatment of the master equation describing the time evolution of the two-level sub-system density matrix beyond a perturbative regime.

We put the emphasis on control scenarios aiming at producing physically relevant processes within the two-level sub-system interacting with its environmental bath. The ultimate goal is to protect against decoherence, the sub-system (such as a qubit), the control taking advantage from memory effects to draw back some information content from the bath to the sub-system. As a first attempt, we consider two targets, namely, the revival of an initial state $|i\rangle$ $(i = 1, 2)$ or a transition between the two states of the sub-system. The optimal control is precisely concerned with these goals through the populations of these states given in terms of the diagonal elements $\rho_{11}(t)$ and $\rho_{22}(t)$ of the sub-system density matrix. Once such control fields have been found, we address the consequences on the bath memory responses. Basically, we observe that non-Markovianity is increased during the optimally driven process. This is actually quantified through some typical signatures: time-dependent behavior of the volume of accessible states displaying bumps during its monotonic decay or the time-dependent behavior of the entropy exhibiting transitory decreases. At that point, we have shown that a control aiming at the protection against decay of the sub-system characteristics provides, as a consequence, higher non-Markovian response of the bath. However, one of the main conclusions is that the mechanism does not necessarily increase the component on the quantum decay channel with the negative rate. We observe in most of the cases a decrease of the weight of the channel with the largest decay rate. Similar behaviors have been obtained for other targets such as the one inducing relaxation towards the ground system eigenstate. The control performances remain however rather modest. The main reasons are the strong system-bath coupling and the limited range of our flash field amplitudes, in relation with their experimental feasibility. To go beyond such limitations, we have to refer to ultra short and intense laser pulses. This requires the introduction of an additional constraint in the optimal control scheme to correct the time integrated pulse area that, following Maxwell equations should be zero [56–58, 59]. Finally, even more realistic calculations should be conducted with *ab initio* transition dipoles, resulting from quantum chemistry codes. An additional challenge would be the relaxation of the system-bath full separability assumption made by the introduction of an initial state through the factorization of the corresponding density matrices, prior to the control. This could presumably be conducted referring to auxiliary matrices resulting from field-free propagation for both initial and target states. According to some results on non-Markovian entanglement dynamics [66], we could expect longer lasting coherence further improving our control efficiency. As mid-term perspectives, future works should deal with exerting control directly on bath dynamics, in such a way to decrease decoherence of the sub-system, or in other words, achieve appropriate control of non-Markovianity to better protect sub-system characteristics. To that end, different strategies can be proposed: (i) additional control of the environment through the introduction of a transition dipole among bath normal modes; (ii) extraction of a collective mode from the bath so as to deal with a control involving an augmented active system, as has already been done in field-free heterojunction [38] or in a SQUID model [24]. We are actively pursuing research of these topics.

Acknowledgments

We acknowledge support from the ANR-DFG COQS, under Grant No. ANR-15-CE30-0023-01. This work has been performed with the support of the Technische Universität München Institute for Advanced Study, funded by the German Excellence Initiative and the European Union Seventh Framework Programme under Grant Agreement No. 291763. This work has also been performed within the French GDR 3575 THEMS.

ORCID iDs

O Atabek https://orcid.org/0000-0002-7510-9946
M Desouter-Lecomte https://orcid.org/0000-0002-6199-7401

References

[1] Weiss U 2012 *Quantum Dissipative Systems* 4th edn (Singapore: World Scientific)
[2] Breuer H-P and Petruccione F 2002 *The Theory of Open Quantum System* (Oxford: Oxford University Press)
[3] de Vega I and Alonso D 2017 *Rev. Mod. Phys.* **89** 015001
[4] Rivas A, Huelga S F and Plenio M B 2014 *Rep. Prog. Phys.* **77** 094001
[5] May V and Kühn O 2011 *Charge and Energy Transfer in Molecular System* (New York: Wiley)
[6] Chin A, Prior J, Rosenbach R, Caycedo-Soler F, Huelga S and Plenio M B 2013 *Nat. Phys.* **9** 113
[7] Lindblad G 1976 *Commun. Math. Phys.* **48** 119
[8] Redfield A G 1965 *Adv. Magn. Res.* **1** 1
[9] Breuer H-P, Laine E M and Piilo J 2009 *Phys. Rev. Lett.* **103** 210401
[10] Breuer H-P, Laine E M, Piilo J and Vacchini B 2016 *Rev. Mod. Phys.* **88** 021003
[11] Lorenzo S, Plastina F and Paternostro M 2011 *Phys. Rev.* A **84** 032124
[12] Hall M J W, Cresser J D, Li L and Anderson E 2014 *Phys. Rev.* A **89** 042120
[13] Anderson E, Cresser J D and Hall M J W 2007 *J. Mod. Phys.* **54** 1695
[14] Haseli S, Salimi S and Khorashad A S 2015 *Quant. Inf. Proc.* **14** 3581
[15] Pötz W 2006 *Appl. Phys. Lett.* **89** 254102
[16] Wenin M and Pötz W 2006 *Appl. Phys. Lett.* **92** 103509
[17] Mancal T and May V 2001 *J. Chem. Phys.* **114** 1510
[18] Beyvers S, Ohtsuki Y and Saalfranck P 2006 *J. Chem. Phys.* **124** 234706
[19] Tremblay J-C and Saalfranck P 2008 *Phys. Rev.* A **89** 063408
[20] Grace M, Brif C, Rabitz H, Walmsley I A, Kosut R I and Lidar D A 2007 *J. Phys. B: At. Mol. Opt. Phys.* **40** S103
[21] Cui W, Xi Z R and Pan Y 2008 *Phys. Rev.* A **77** 032117
[22] Pachón L A and Brumer P 2013 *J. Chem. Phys.* **139** 164123
[23] Tai J-S, Lin K-T and Goan H-S E 2014 *Phys. Rev.* A **89** 062310
[24] Reich D M, Katz N and Koch C P 2015 *Sci. Rep.* **5** 12430
[25] Poggi P M, Lombardo M C and Wisiacki D A 2017 *Europhys. Lett.* **118** 20005
[26] Glaser S J *et al* 2015 *Eur. Phys. J.* D **69** 279
[27] Koch C P 2016 *J. Phys.: Condens. Matter* **28** 213001
[28] Addis C, Maine E-M, Gneiting C and Maniscalco S 2016 *Phys. Rev.* A **94** 052117
[29] Puthumpally-Joseph R, Atabek O, Mangaud E, Desouter-Lecomte M and Sugny D 2017 *Mol. Phys.* **115** 1944
[30] Puthumpally-Joseph R, Mangaud E, Desouter-Lecomte M, Sugny D and Atabek O 2018 *Phys. Rev.* A **97** 033411
[31] Basilewitsch D, Schmidt R, Sugny D, Maniscalo S and Koch C P 2017 *New J. Phys.* **19** 113042
[32] Tannor D J and Rice S A J 1985 *J. Chem. Phys.* **83** 5013
[33] Shapiro M and Brumer P J 1986 *J. Chem. Phys.* **84** 4103
[34] Kosloff R, Rice S A, Gaspard P, Tersigni S and Tannor D J 1989 *Chem. Phys.* **139** 201
[35] Leggett A J, Chakravarty S, Dorsey A T, Fisher M P A, Garg A and Zwerger W 1987 *Rev. Mod. Phys.* **59** 1
[36] Tamura H, Burghardt I and Tsukada M 2011 *J. Phys. Chem.* C **115** 10205
[37] Tamura H, Martinazzo R, Ruckenbauer M and Burghardt I 2012 *J. Chem. Phys.* **137** 22A540
[38] Mangaud E, Meier C and Desouter-Lecomte M 2017 *Chem. Phys.* **494** 90
[39] Caruso F, Montangero S, Calarco T, Huelga S F and Plenio M B 2012 *Phys. Rev.* A **85** 042331
[40] Hoyer S, Caruso F, Montangero S, Soravar M, Calarco T, Plenio M B and Whaley K B 2014 *New J. Phys.* **16** 045007
[41] Tanimura Y and Kubo R 1989 *J. Phys. Soc. Japan* **58** 101
[42] Ishizaki A and Tanimura Y 2005 *J. Phys. Soc. Japan* **74** 3131
[43] Tanimura Y 2006 *J. Phys. Soc. Japan* **75** 082001
[44] Xu R-X and Yan Y 2007 *Phys. Rev.* E **75** 031107
[45] Strümpfer J and Schulten K 2012 *J. Chem. Theory Comput.* **8** 2808
[46] Kreisbeck C, Kramer T and Aspuru-Guzik A 2014 *J. Chem. Theory Comput.* **10** 4045
[47] Ohtsuki Y, Zhu W and Rabitz H 1999 *J. Chem. Phys.* **110** 9825
[48] Ohtsuki Y 2003 *J. Chem. Phys.* **119** 661
[49] Ohtsuki Y, Turinici G and Rabitz H 2004 *J. Chem. Phys.* **120** 5509
[50] Xu R, Yan Y, Ohtsuki Y, Fujimura Y and Rabitz H 2004 *J. Chem. Phys.* **120** 6600
[51] Korolkov M V, Manz J and Paramorov G K 1996 *J. Chem. Phys.* **105** 10874
[52] Sugny D, Ndong M, Lauvergnat D, Justum Y and Desouter-Lecomte M 2007 *J. Photochem. Photobiol.* A **190** 359
[53] Chenel A, Dive G, Meier C and Desouter-Lecomte M 2012 *J. Phys. Chem.* A **116** 11273
[54] Krauss K 1983 *States, Effects and Operations: Fundamental Notions of Quantum Theory* (Berlin: Springer)
[55] Alicki R and Lendi K 2007 *Quantum Dynamical Semigroups and Applications* (Berlin: Springer)
[56] Brabec T and Krausz F 2000 *Rev. Mod. Phys.* **72** 545
[57] Dion C M, Keller A and Atabek O 2001 *Eur. Phys. J.* D **14** 249
[58] Bandrauk A D, Barnaki S, Chelkowski S and Kamta G L 2006 *Progress in Ultrafast Intense Laser Science* ed K Yamanouchi *et al* vol 3 (Berlin: Springer)
[59] Sugny D, Vranckx S, Ndong M, Vaeck N, Atabek O and Desouter-Lecomte M 2014 *Phys. Rev.* A **90** 053404
[60] Zhu L, Liu H, Xie W and Shi Q 2012 *J. Chem. Phys.* **137** 194106
[61] Laine E-M, Piilo J and Breuer H-P 2010 *Europhys. Lett.* **92** 60010
[62] Ringbauer M, Wood C J, Modi K, Gilchrist A, White A G and Fedrizzi A 2015 *Phys. Rev. Lett.* **114** 090402
[63] Modi K 2012 *Sci. Rep.* **2** 581
[64] Burghardt I 2001 *J. Chem. Phys.* **114** 89
[65] Pomyalov A, Meier C and Tannor D J 2010 *Chem. Phys.* **370** 98
[66] Dijkstra A G and Tanimura Y 2010 *Phys. Rev. Lett.* **104** 250401
[67] Meier C and Tannor D J 1999 *J. Chem. Phys.* **111** 3365
[68] Werschnick J and Gross E K U 2007 *J. Phys. B: At. Mol. Opt. Phys.* **40** 175